Electronic and structural properties of RuO_2

Keith M. Glassford and James R. Chelikowsky
Department of Chemical Engineering and Materials Science and Minnesota Supercomputer Institute, University of Minnesota, Minneapolis, Minnesota 55455
(Received 26 May 1992)

We present *ab initio* total-energy calculations for the cohesive, structural, and electronic properties of RuO_2 in the rutile structure. Our calculations were performed within the local-density approximation employing "soft-core" *ab initio* pseudopotentials and a plane-wave basis. Our calculated cohesive energy and structural parameters are within 10% and 2% of experimental values, respectively, as is typical of local-density calculations. We find good agreement between our theoretical density of states and experimental photoemission results and predict a Fermi surface which agrees well with experiment. Our results for this late transition-metal oxide show that the local-density approximation yields accurate electronic and structural properties for a "weakly magnetic" system.

I. INTRODUCTION

Ruthenium dioxide crystallizes in the rutile structure and exhibits metallic conductivity at room temperature[1] resulting from the partially filled Ru $4d$ states. RuO_2 has found use as a selective catalyst in the oxidation of methane to synthesis gas,[2] in ceramic resistors,[3] electrochemical capacitors,[4] and in the catalytic photodecomposition of water.[5] Its major technical application, however, resides in the chlor-alkali industry as an electrocatalyst in the evolution[6-8] of Cl_2, and to a lesser extent in the evolution[9,10] of O_2 and H_2. Increasing the long-term stability and electrocatylitic activity of anodic and cathodic electrodes has been an ongoing research problem in electrochemistry and electrochemical engineering. The most successful approach has been the development of "dimensionally stable anodes" (DSA) in the mixed oxide system $Ru_xTi_{1-x}O_2/Ti$, which we are currently examining.

We have chosen to study RuO_2 for a variety of reasons: Very few *ab initio* pseudopotential calculations have been performed for late transition-metal oxides within the local-density approximation. By comparing to experimental results and previous self-consistent all-electron calculations we can determine the ability of the pseudopotential plane-wave formalism in predicting accurate structural and electronic properties for these complex systems. Furthermore, the electronic and structural properties of RuO_2 are important toward understanding the catalytic and electronic properties of the $Ru_xTi_{1-x}O_2$ system as well as mixed oxide systems in general.

Although a technically important oxide, very little theoretical or experimental work has been performed on RuO_2 as compared to, say, TiO_2.[11] The electronic properties for RuO_2 have been experimentally probed by Fermi-surface (FS) measurements,[12-15] x-ray and ultraviolet photoelectron spectroscopic studies,[9,16-19] and reflectivity experiments.[20] The first theoretical calculations were performed by Mattheiss[21] using a tight-binding approach based on non-self-consistent augmented-plane-wave linear combination of atomic orbitals (APW-LCAO) calculations. These calculations are generally in good agreement with photoemission[9,16-19] and Fermi-surface measurements.[12] However, the separation found in these calculations between the O $2p$–Ru $4d$ manifolds is larger than expected owing to an overestimation in the covalent character between these states.[21] Experimental reflectivity measurements[20] find good agreement with the theoretical results of Mattheiss[21] if the O $2p$ bands are shifted towards the Fermi level by ~ 1 eV, and matrix element effects are neglected. Recently, Xu, Jarlborg, and Freeman[22] have performed self-consistent semirelativitic linear muffin-tin orbital (LMTO) calculations for the rutile oxides RuO_2, IrO_2, and OsO_2. As expected, self-consistency is important in positioning the O $2p$ bands as significant charge transfer takes place in metallic oxides. Self-consistent full-potential linearized augmented plane-wave (FLAPW) calculations have also been recently performed by Sorantin and Schwarz[24] for a number of transition-metal oxides. Their results are in good agreement with the LMTO calculations for RuO_2 as well as our previous pseudopotential calculations for TiO_2.[11] Recent photoemission experiments by Daniels *et al.*[18] favor a large p-d gap, in agreement with the calculations of Mattheiss,[21] but conflicting with earlier photoemission results.[16,17,9] These earlier experiments, favoring a smaller p-d gap, agree with recent LMTO,[22] augmented-spherical-wave (ASW),[23] and FLAPW[24] calculations.

In the present study, we use a different approach in calculating the electronic properties of RuO_2 as well as performing total-energy calculations to determine the ground-state properties and pressure-induced variations in the structural parameters. We self-consistently solve the Hohenberg-Kohn-Sham[25] (HKS) equations within the local-density approximation (LDA) using *ab initio* pseudopotentials.[31,32] This approach has been very successful in predicting ground-state structural, cohesive, and elastic properties of condensed-matter systems.[26] The method yields lattice constants, bulk moduli, elastic constants, and phonon frequencies usually within 1–5 % of experimental values.[27] For binding energies, the LDA

typically overestimates the experimental values by approximately 15–20% as a result of cancellation errors occurring within the LDA.[28,26]

Recent studies have focused on the validity[29] of the LDA in calculating the electronic properties of late transition-metal oxides. An inherent difficulty with these systems, e.g., FeO and CoO, is the ability to separate magnetic effects from those due to cancellation errors within the LDA. Owing to its weak Pauli paramagnetic behavior, RuO_2 provides an example of a late-transition-metal-bearing oxide for which magnetic effects may be neglected. By performing total-energy calculations we can compare our theoretically determined structural, cohesive, and electronic properties to experimental results and we may assess the ability of the LDA to predict these properties on a fundamental level.

Calculating the electronic properties of transition-metal oxides from "first principles" has traditionally been a computationally demanding problem. Until recently, it has been impractical to perform total-energy calculations for the majority of transition-metal oxides using a plane-wave basis. Unlike simple metals or semiconductors, the valence d states of transition metals are localized near the core region. This results in poor convergence when a modest number of plane waves is used in conjunction with traditional pseudopotentials.[30] For transition-metal oxides, further complications exist as the O $2p$ valence wave functions have no corresponding core states of the same angular momentum. Since the O $2p$ state need not be orthogonal to the core, such states are localized in contrast to second-row elements such as sulfur. With the recent advances in methods for generating "soft-core" transferable pseudopotentials[31,32] and more efficient computational techniques[30,33,34] we are in a position to handle these complex systems from a first-principles approach.

The remainder of the paper is outlined as follows. A brief summary of our calculational method is given in Sec. II. In Sec. III we examine the structural and cohesive properties of RuO_2 in the rutile structure, investigate changes in the structural parameters under pressure, and compare our *ab initio* results to experiment. In Sec. IV we discuss the electronic properties, examine the band structure, electronic density of states, and Fermi surface. In this section we also investigate the charge transfer from Ru to O in terms of the pseudovalence charge-density difference maps in various high-symmetry planes of the tetragonal lattice. We end in Sec. V with a summary of our results.

II. METHODS OF CALCULATION

The structural and electronic properties of RuO_2 have been calculated within the LDA using *ab initio* pseudopotentials and a plane-wave basis in conjunction with a fast iterative diagonalization technique.[30,33,34] This approach has recently been shown to give good results for the electronic, structural, and optical properties of TiO_2, which also forms in the rutile structure.[35,11] Our Ru pseudopotential was relativistically generated in the atomic ground-state configuration ($5s^1 4d^7 4p^0$) using the method of Troullier and Martins.[31] The exchange-correlation potential of Ceperly and Adler[36] as parametrized by Perdew and Zunger[37] has been used. A core radius of 2.7 a.u. was chosen for the s, p, and d components of the pseudopotential. Our pseudopotential, averaged over $j\pm\frac{1}{2}$ states, includes relativistic effects to order α^2, where α is the fine-structure constant.[38] The resulting pseudopotential was transformed using the method of Kleinman and Bylander[39] with the s component chosen as the local potential. This procedure leads to a "soft" pseudopotential with good transferability over a wide energy range. We have verified that our choice of core radii and local pseudopotential component for the Kleinman and Bylander operator did not result in the appearance of any ghost states.[40] Our O pseudopotential is identical to that given in previous calculations for TiO_2.[11]

We have included plane waves up to an energy cutoff of 64 Ry. At equilibrium our basis set consists of $\sim$3700 plane waves. Increasing this cutoff to 100 Ry decreased the total energy per unit cell by only 18 mRy. In the case of metals such as RuO_2, one typically needs a large number of $\mathbf{k}$ points to achieve convergence in the total energy as well as a large number of iterations to reach self-consistency. This is largely due to oscillations in the self-consistency cycle of the charge between the oxygen and metal atoms. To circumvent this problem, we have implemented the Gaussian broadening scheme of Fu and Ho[41] to account for variations in the metal band occupancies near the Fermi level. We used a Gaussian width of 0.01 Ry. A total of six special $\mathbf{k}$ points were used in calculating the structural and electronic properties. We have tested our $\mathbf{k}$-point sampling by increasing to 18 special $\mathbf{k}$ points: the total energy increased by only 0.02 eV/atom. Self-consistency was determined by a maximum difference of 0.01 mRy between input and output Fourier components of the screening potential. This difference corresponds to total energies which are stable to within $\sim 10^{-6}$ Ry.

III. STRUCTURAL AND COHESIVE PROPERTIES

Ruthenium dioxide crystallizes in the rutile structure with space-group symmetry $P4_2/mnm$ (D_{4h}^{14}), as is common of many transition-metal dioxides.[42] The tetragonal Bravais lattice contains two RuO_2 molecules per primitive cell and is illustrated in Fig. 1. The two Ru atoms occupy the Wycoff $2(a)$ sites, $(0,0,0;\frac{1}{2},\frac{1}{2},\frac{1}{2})$, while the four O atoms occupy the $4(f)$ sites, $\pm(u,u,0;u+\frac{1}{2},\frac{1}{2}-u,\frac{1}{2})$, where u is an internal parameter and along with a and c/a describe the oxygen octahedra surrounding each Ru atom. In Fig. 1 we illustrate the oxygen octahedra surrounding the central Ru atom by dashed lines. These octahedra form edge-shared chains running parallel to the c axis. Distortions away from perfect octahedral symmetry are typically measured in terms of the ratio of the apical and equatorial metal-oxygen bond lengths, d_a/d_e, which is equal to 1 for a regular octahedron. In the rutile structure the two apical bonds are of length $au\sqrt{2}$ while the four equatorial bonds are of length $a[2(2u-1)^2+(c/a)^2]^{1/2}/2$. From the experimental lattice constants[43] of RuO_2 one finds an apical-to-equatorial ratio of 0.979, indicating a compression of the

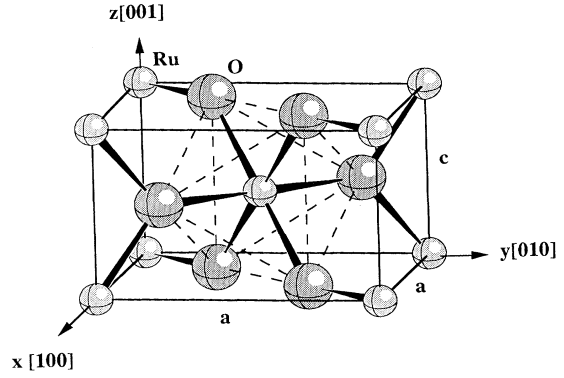

FIG. 1. Primitive unit cell for RuO_2 in the rutile structure. The dashed lines illustrate the connectivity of the oxygen octahedra for the central Ru atom.

octahedron along its principal axis, i.e., the $[1\bar{1}0]$ direction in Fig. 1. In the case of TiO_2, the situation is reversed in that the apical bond length is $\sim 2\%$ larger than the equatorial. Further discussion of the structural properties of various rutile oxides has been reviewed by Sorantin and Schwarz.[24] Early studies on the determination of the crystal structure have been reviewed by Trasatti and O'Grady.[7]

First-principles calculations were performed to determine the structural parameters a, c, and u of RuO_2, in the $P4_2/mnm$ structure. This is achieved by minimizing the total energy of the unit cell at given volumes and fitting the theoretical values of energy and volume to the Birch-Murhagnan[44] integrated equation of state (EOS). At each volume $V=ca^2$ we perform a constrained total-energy minimization with respect to c/a and u. In Fig. 2 we show the values of a, c, and u which minimize the total energy at specific volumes using the above prescription. The corresponding energy-volume relationship is illustrated in Fig. 3. The cohesive energy E_{coh} is defined as the difference between the total energy of the solid and the isolated "pseudoatoms." The cohesive energy and unit cell volume in Fig. 3 are based on a single RuO_2 molecule. From our pseudopotential calculations, we find the energy of the isolated pseudoatoms to be -429.59 and -433.43 eV for O and Ru, respectively. These values include a spin-polarization correction[45] of 1.41 and 1.62 eV for O and Ru, respectively, using the corresponding spin-polarized exchange-correlation potentials.[36,37]

In Table I we compare our theoretically determined structural, elastic, and cohesive properties to experimental results. Our structural parameters are within 2% of the experimental values.[46,43] This is expected as structural properties are typically insensitive to errors within the LDA, i.e., one is taking differences between solid phases where the cancellation of errors is usually quite good. However, for cohesive energies which do not involve differences between solid phases, incomplete cancellations associated with the LDA become more important, resulting in cohesive energies which are frequently 15–20% larger than experiment.[28,26] This is the case in the present calculations, where we find a cohesive energy which is approximately 10% larger than experiment. The experimental cohesive energy reported in Table I was calculated using a heat of formation for RuO_2 of -72.90 kcal/mol,[47] a cohesive energy for Ru of 155.42

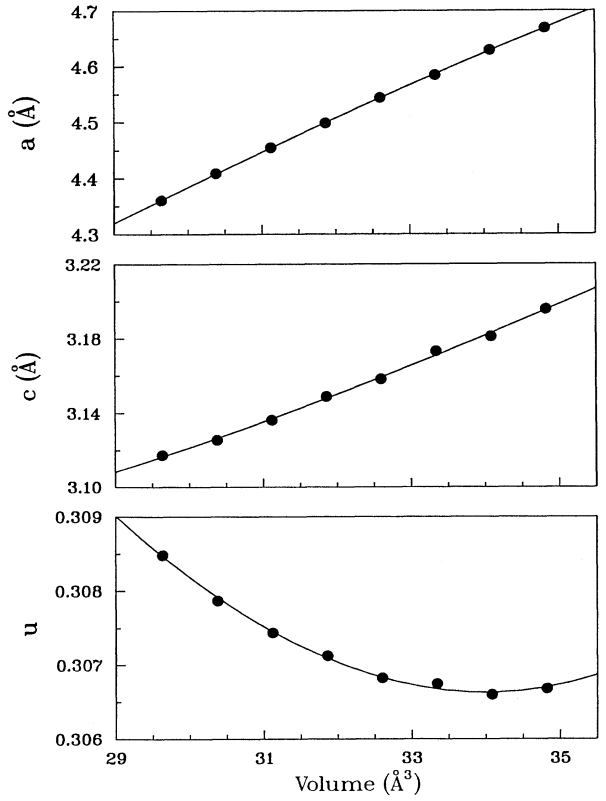

FIG. 2. Structural parameters a, c, and u for RuO_2 in the rutile structure obtained from *ab initio* total-energy calculations for various volumes, the volume being per RuO_2 molecule unit. Calculated points are illustrated by solid circles while the line represents a guide to the eye.

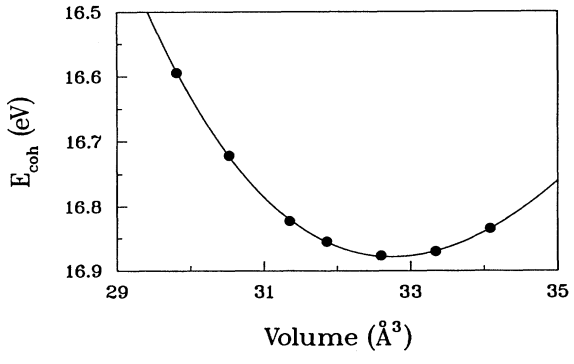

FIG. 3. Theoretical equation of state for RuO_2 in the rutile structure fitted to the Birch-Murnaghan (Ref. 44) integrated equation of state (solid line) and the corresponding theoretically values (solid circles). Cohesive energies and volume are per RuO_2 molecule.

TABLE I. Comparison of the experimentally determined structural (Ref. 43), cohesive (Ref. 47), and elastic parameters (Ref. 46) for RuO_2 in the rutile structure with the present theory. See text for nomenclature.

Property	Theory	Experiment
E_{coh} (eV/RuO_2)	16.89	15.07
V_0 (Å^3/RuO_2)	32.8	31.24
a (Å)	4.56	4.492
c (Å)	3.16	3.106
c/a	0.694	0.692
u	0.3068	0.3058
B_0 (GPa)	283	270
B_0'	4.6	4
$\beta_\perp$ (10^{-3} GPa^{-1})	1.5	1.5
$\beta_\parallel$ (10^{-3} GPa^{-1})	0.59	0.6

kcal/mol,[48] and a dissociation energy for O_2 of 119.1 kcal/mol.[47] We have not considered thermal or vibrational contributions to the structural and cohesive properties as these are expected to be less than the inherent errors from the LDA.

The equilibrium bulk modulus B_0 and its pressure derivative B_0' were determined from the integrated Birch-Murhagnan EOS.[44] We find an isothermal bulk modulus of 283 GPa and an equilibrium pressure derivative of 4.6. The experimental situation is somewhat unclear as the values of B_0 and B_0' were obtained from a limited set of low-pressure data[46] where B_0' was fixed at 4, resulting in a B_0 value of 270 GPa. Using the experimental data,[46] we found that changes in B_0' by ± 1 resulted in changes in B_0 by only ∓ 1 GPa. Given the experimental uncertainties, our theoretical values are in good agreement with experiment. We have examined the changes in the structural properties under hydrostatic pressure. In Fig. 4 we illustrate the dependence of the lattice parameters a and c on the unit-cell volume. To enhance trends in the structural parameters, we have normalized the theoretical and experimental[46] values by their equilibrium values. As seen in Fig. 4, good agreement with the experimentally determined pressure-induced structural changes are obtained. This agreement is also reflected in the bulk linear compressibilities perpendicular, $\beta_\perp = -d \ln a/dP$, and parallel, $\beta_\parallel = -d \ln c/dP$, to the c axis. The resulting linear compressibilities are given in Table I and are in good agreement with low-pressure experiments of Hazen and Finger.[46] We find a large anisotropy in the linear compressibilities, $\beta_\perp/\beta_\parallel$, of 2.5, in agreement with the experimental value of 2.6. The anisotropy can be traced to the insensitivity of c to volume or pressure changes, as seen in Fig. 2. We also find an increase in u under pressure (Fig. 2), as experiment suggests.

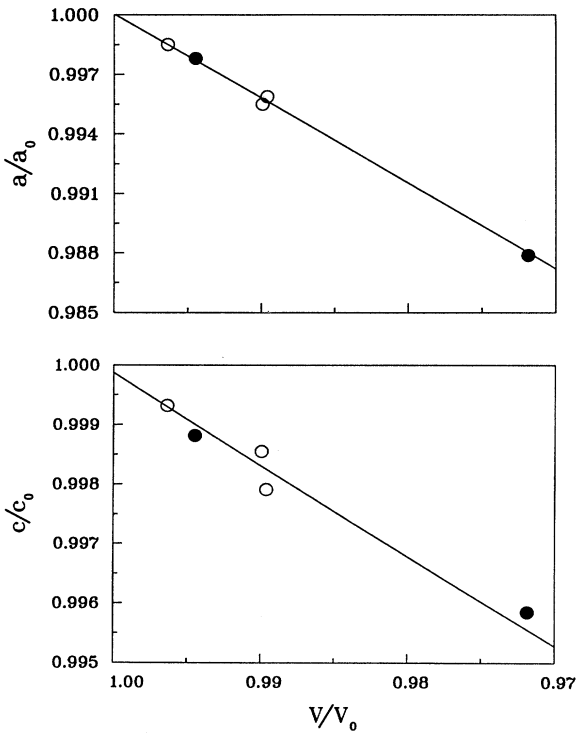

FIG. 4. Comparison of pressure-induced variations in the structural parameters a and c compared to experimental results. Solid circles represent the present results and open circles represent the experimental results of Hazen and Finger (Ref. 46). The solid line is intended only as a guide to the eye and corresponds to that illustrated in Fig. 2.

IV. ELECTRONIC PROPERTIES

The self-consistent band structure for RuO_2 is shown in Fig. 5 along the high-symmetry directions of the Brillouin zone (BZ), which is subsequently shown in Fig. 6. In Fig. 7 we show the corresponding density of states (DOS) as calculated by the linear analytic tetrahedron method[49] with self-consistent eigenvalues determined at 126 **k** points in the irreducible BZ. The Fermi energy E_F calculated from the integrated DOS was found to be in excellent agreement (a difference of only 0.01 eV) with that obtained using the weighting scheme discussed in Sec. II. In both of these figures, we have taken E_F as our energy zero.

The O 2s bands, shown in the lower panel of Fig. 5, have a bandwidth of 2.7 eV and are approximately 18.5 eV from the Fermi level. As seen in Table II, the location of the O 2s feature is in good agreement with previous LDA calculations[22,24] to within a few tenths of an eV. The theoretical LDA values are, however, approximately 3 eV underbound when compared to experiment (Table II). This difference is probably a combination of errors occurring within the LDA, experimental resolution, and electronic relaxation effects, the latter typically being approximately 1 eV. Notwithstanding, we obtain fairly good agreement with experimental[16,9] values in the range 21.1–22 eV. The next 12 bands are predominantly O 2p in character with a bandwidth of 6.8 eV, the lower edge of these states being approximately 8.4 eV below the Fermi level. This is in good agreement with experimental x-ray photoelectron spectroscopy (XPS) measure-

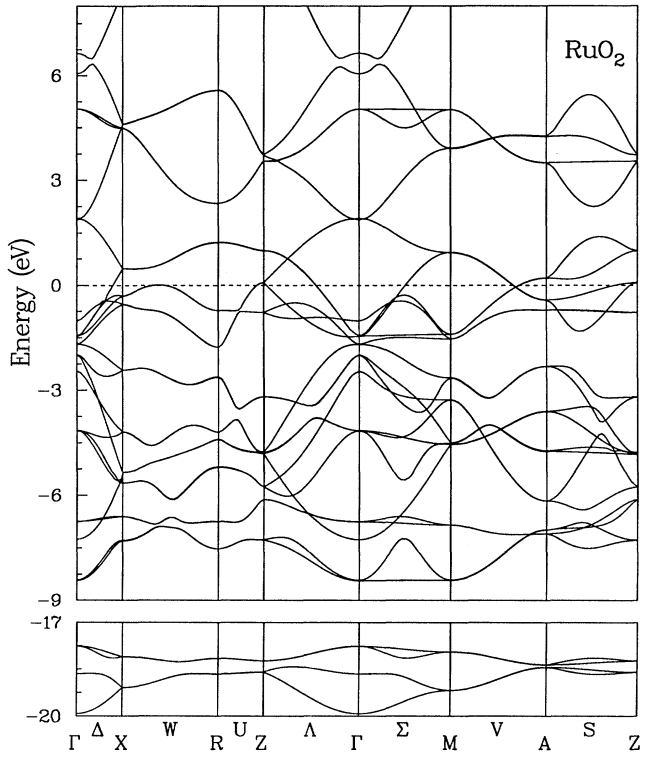

FIG. 5. Band structure for RuO_2 along high-symmetry directions of the irreducible Brillouin zone. The energy zero has been taken at the Fermi energy.

ments,[16,17,9] which find the O 2*p* band edge at approximately 9 to 10 eV below the Fermi level and a bandwidth of approximately 7 to 8 eV. In Table III, we compare our bandwidths for various features in the valence and conduction bands to previous theoretical calculations. Our O 2*p* width is within a few tenths of an eV of previous self-consistent calculations. We note that the O 2*s* width is little under 1 eV larger than previous self-consistent calculations[23,22,24] but is more in line with the experimental[16,9] values around 4.5 to 5.5 eV. We attribute the majority of this difference to experimental resolution and tailing effects due to lifetime broadening[50] rather than LDA.

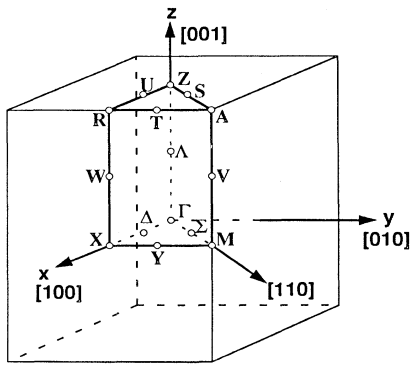

FIG. 6. Symmetry labels for the irreducible Brillouin zone of the tetragonal Bravais lattice.

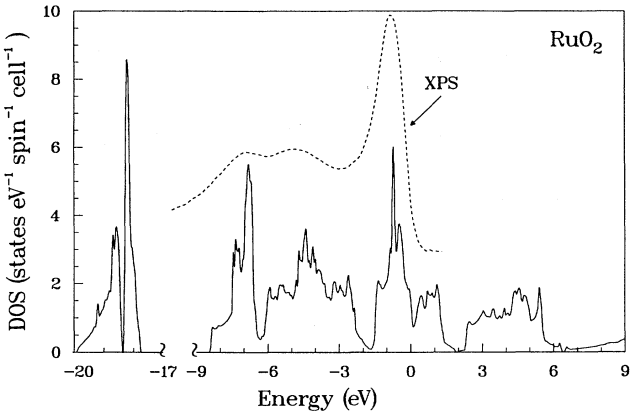

FIG. 7. Theoretical density of states for RuO_2 (solid line) in states eV^{-1} $cell^{-1}$ $spin^{-1}$ compared to experimental XPS measurements (arb. units) by Riga *et al.* (Ref. 16) (dashed line). The Fermi energy has been taken as the energy zero.

In Fig. 7 we compare our theoretical valence-band DOS to the experimental XPS measurements of Riga *et al.*[16] The two major peaks in the O 2*p* manifold is characteristic of most octahedrally coordinated transition-metal oxides and may be attributed to metal-oxygen σ- and π-bonding states. As seen in our DOS of Fig. 7, we find a σ-π separation between the major σ peak and the central π peak of approximately 2.6 eV (see Table II). This separation is consistent with previous theoretical calculations and is in fairly good agreement with experimental XPS (Refs. 16 and 17) results in the range 1.9–2.1 eV. However, a direct comparison between theory and experiment is not entirely correct as matrix element effects tend to shift peak intensities. Further modifications occur due to differences in the partial photoabsorption cross sections between the O 2*p* and Ru 4*d* states with XPS radiation, the Ru 4*d* cross section being approximately 30 times greater than the O 2*p*.[51] In the case of RuO_2, previous theoretical calculations[21,23] reveal only minor Ru 4*d* character in the vicinity of the O 2*p*-π manifold. Furthermore, the location of the peaks in the partial DOS for *d* and *p* electrons were found to be approximately coincident. Features observed in XPS should therefore reflect the major O 2*p* states with only minor shifts resulting from matrix element effects. This has been confirmed by the LMTO calculations of Xu, Jarlborg, and Freeman,[22] who find that inclusion of matrix element effects, ignoring electronic relaxations, is in good agreement with the experimental XPS (Ref. 16) measurements shown in Fig. 7. Our peak positions and bandwidths are in good agreement with the XPS measurements,[16] where the experimental O 2*p*-π state is shifted by approximately 0.3 eV to lower binding energies as a result of matrix element effects (Table II).

To increase the probability of scattering of O 2*p* states, Daniels *et al.*[18] performed ultraviolet photoemission

TABLE II. Comparison of peak positions, in eV below E_F, for various spectral features in the conduction band. Column headings indicate the major character of the resulting manifolds and are only for labeling purposes. Three peaks in the theoretical O $2p$-π manifold, when observed, reflect the center of gravity of those seen in Fig. 7. A direct comparison between theoretical and experimental peak positions in the O $2p$ manifold is not implied, as matrix element effects will modify the theoretical peak positions.

O $2s$	O $2p$-σ	O $2p$-π	Ru t_{2g}	Method	Ref.
18.5	7.0	5.7, 4.4, 2.8	0.7	Present	Present
18.3	7.2	5.6, 4.2, 2.8	0.9	FLAPW	24
18.6	7.0	5.5, 4.5, 3.1	0.7	ASW	23
18.7	7.0	4.6	0.54	LMTO	22
20.3	6.8	5.6, 4.8, 3.5	0.5	APW-LCAO	21
21.1	6.9	4.7	0.6	XPS	16
22.0	7.1	5.2	0.8	XPS	9
	7.4	5.8, 3.8	1.2	UPS	18
		4.8	0.55	UPS	19
	7.0	4.7	0.6	XPS	19
	7.0	4.7	1.4	XPS	17
			0.68	UPS	17

spectroscopic (UPS) experiments for photon energies in the range $70 \leq \hbar\omega \leq 130$ eV. In this region the O $2p$ cross section is approximately three times larger than that of Ru $4d$.[51] The O $2p$ states should dominate the spectra, unlike He I UPS spectra,[19,17] where the Ru $4d$ cross section is approximately three times larger than that of the O $2p$.[51] As expected, they observe one additional feature at 3.8 eV and tentatively assigned it to a lower binding energy shoulder of the main π-bonding peak which results from the symmetry lowering of the metal sites from $O_h \rightarrow D_{2h}$. The authors have also considered changes in the valence-band structure for the complex oxide $Ru_xIr_{1-x}O_2$ for $0 \leq x \leq 1$. They find the t_{2g} peak, labeled A in their paper, to be insensitive to variations in x. This result has not been reproduced by recent XPS experiments by Kötz and Stucki;[9] rather they find the t_{2g} peak to shift by 1 eV on going from RuO_2 to IrO_2, indicating a higher affinity of oxygen for Ru than for Ir.[9] Another discrepancy in the UPS results of Daniels *et al.*[18] and other photoemission experiments[9,16,17,19] is their large valence-band width, which is approximately 2 eV larger than other experiments. However, it is difficult to interpret from their result where the band edge ends and the secondary background takes over.

The next ten bands from approximately 2.5 to 6 eV illustrated in Fig. 5, and reflected in the DOS of Fig. 7, are predominantly of d character. For transition-metal oxides in which the metal atoms are octahedrally coordinated, these states are often interpreted in terms of the octahedral crystal-field splitting of the fivefold-degenerate d states into the triply degenerate t_{2g} and doubly degenerate e_g states. In the $P4_2/mnm$ space group, distortions away from perfect O_h symmetry lower the metal-atom site symmetry to D_{2h}, resulting in further splitting of these states into singly degenerate levels. As the distortion away from O_h symmetry is small in RuO_2, we will maintain the t_{2g}-e_g nomenclature of the O_h group owing to its simplicity.

Of the first ten metal-atom d bands, the first six are associated with the t_{2g} manifold having a bandwidth of 3.6 eV, while the next four bands are associated with the e_g manifold with a bandwidth of 4.5 eV. These two sets of bands are well separated throughout the BZ except at Γ, where they touch. The Fermi level, indicated by the dashed line in Fig. 5, is located approximately midway between the t_{2g} manifold and is approximately 1.7 eV from its lower edge. This is in good agreement with UPS experiments,[19] which place the lower edge of the t_{2g} manifold at approximately 1.5 eV below E_F. Bands 19–21 are found to intersect the Fermi surface forming one electron and two hole sheets and will be discussed below. We note that the doubly degenerate bands 19 and 20 along W are nearly degenerate with the Fermi energy. The main

TABLE III. Comparison of widths, in eV, of various valence-band and conduction-band manifolds between different theoretical calculations. Column headings indicate the major character of the resulting manifolds.

O $2s$	O $2p$	Ru t_{2g}	Ru e_g	Method	Ref.
2.7	6.8	3.6	4.5	Present	Present
1.9	6.5	3.2	3.8	FLAPW	24
2.1	6.3	3.4	4.1	ASW	23
	6.5	3.4	3.6	LMTO	22
1.4	5.1	2.3	3.7	APW-LCAO	21

peak in the DOS for these occupied bands is approximately 0.7 eV below E_F and is largely attributed to rather dispersionless bands in the S, W, and V directions. This separation is in good agreement with photoemission results[16,9,17,19] of 0.5 to 0.8 eV, ASW calculations,[23] LMTO calculations[22] of 0.54 eV, and APW-LCAO calculations[21] of 0.8 eV. The top band shown in Fig. 5 is primarily of Ru sp character. The separation between the Ru sp states and the top of the e_g manifold is similar to that found in calculations for TiO_2.[11]

Overall we find good agreement between the present *ab initio* pseudopotential results and previous all-electron LMTO (Ref. 22) and FLAPW (Ref. 24) calculations. These self-consistent calculations reveal a gap of approximately 0 to 0.3 eV between the O $2p$ and Ru t_{2g} band complexes, confirming the overestimated covalent character in the APW-LCAO calculations of Mattheiss.[21] Other than these shifts and some minor changes in bandwidths (Table III), the initial calculations of Mattheiss[21] are in good agreement with the self-consistent calculations. According to our LDA results, as well as LMTO,[22] FLAPW,[24] and ASW (Ref. 23) calculations, a large p-d gap is not the cause for the large valence-band width seen in the photoemission results of Daniels *et al.*[18]

As seen in Fig. 7, the density of states at the Fermi energy, $D(E_F)$, is near the minimum of the t_{2g} manifold. This low value of $D(E)$ at the Fermi surface has been linked to the stability of RuO_2 against metal-atom pairing along the c axis, as in the rutile form of VO_2 where E_F lies in the middle of the e_g manifold.[19,24] From our DOS shown in Fig. 7, we find a value of $D(E_F)$ of 1.7 states eV^{-1} $cell^{-1}$ $spin^{-1}$, which is in fairly good agreement with the experimental value of 2.1 obtained from high-resolution He I UPS experiments by Cox *et al.*[19] Our value of $D(E_F)$ agrees well with the theoretical calculations of Schwarz[23] and Mattheiss[21] of 1.69 and 1.89 states eV^{-1} $cell^{-1}$ $spin^{-1}$, respectively, but are notably smaller than the value of 2.89 obtained from the LMTO calculations.[22] It should be stressed, however, as seen from Fig. 7, that a small shift in E_F may result in a substantial shift in $D(E_F)$. An indirect comparison of our $D(E_F)$ may also be made via the Sommerfeld coefficient of specific heat, γ, which is proportional to $D(E_F)$. Using our value of $D(E_F)$, we find a γ of 3.98 mJ mol^{-1} deg^{-2}. The experimental[52] coefficient of specific heat due to conduction electrons is 5.77 mJ mol^{-1} deg^{-2}, indicating an effective mass ($\gamma_{expt}/\gamma_{theor}=m^*/m_e$) of 1.4.

Another test of our band-structure calculations is in the comparison of our theoretical Fermi surface with experimental results. The Fermi surface has been experimentally probed by magnetothermal oscillations,[12] magnetoresistance,[14] Azbel-Kaner cyclotron resonance,[13] and de Haas–van Alphen measurements.[15] These experiments provide information on the nature of the electron orbits under the influence of an applied magnetic field, i.e., open or closed orbits. In the case of closed orbits, cross-sectional areas, or their derivatives, in planes perpendicular to the magnetic field are obtained,[53] allowing a detailed comparison with our theoretical Fermi surface.

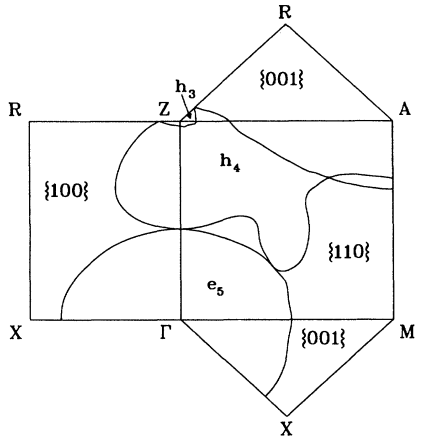

FIG. 8. Intersections of the theoretical RuO_2 Fermi surface with the high-symmetry planes of the irreducible BZ.

In Fig. 8 we show intersections of the Fermi surface with the high-symmetry planes of the irreducible BZ. The fifth t_{2g} band forms a spherically distorted electron sheet e_5 centered at Γ. The fourth t_{2g} band forms a hole sheet h_4 with arms in the $\{110\}$ planes. The third t_{2g} band forms a hole sheet h_3 centered at Z. In the case of the experimental measurements only cross-sectional areas for extremal orbits are obtained. While a detailed mapping of the Fermi surface for RuO_2 has not been performed, our results are in good agreement with the empirical model proposed by Graebner, Greiner, and Ryden[12] based on experimental magnetothermal oscillations. In Table IV we compare our theoretical areas for extremal orbits of the e_5 Fermi sheet centered at Γ with the experimental results of Graebner, Greiner, and Ryden.[12] In calculating the cross-sectional areas, we have assumed that spin-orbit splitting will lift the degeneracy between sheets e_5 and h_4 along Δ without any major shift in the topology of the Fermi sheets.[21] We do not assume the extremal orbits are spherical as in previous calculations.[22] We fitted the radii as function of the subtended angle, and performed the iterated integral. As can be seen in Table IV, our cross-sectional areas are in good agreement with experiment,[12] and are within 5% of the experimental values or better. We have not attempted to calculate the cross-sectional areas for the other sheets owing to their low symmetry.

The major differences between our FS and the empirical model of Graebner, Greiner, and Ryden[12] occurs at

TABLE IV. Cross-sectional areas ($Å^{-2}$) for the Fermi sheet e_5 centered at Γ for magnetic fields perpendicular to high-symmetry planes compared to experimental areas determined from magnetothermal oscillations by Graebner, Greiner, and Ryden (Ref. 12).

Plane	Theory	Experiment
{001}	0.885	0.9317
{100}	0.796	0.8206
{110}	0.755	0.7776

the neck centered at Z, and the arms in the {110} direction. The experimental results find the intersection of the FS in the {110} plane along S to be degenerate with zero slope. Similar results have been found from LMTO calculations.[22] Examination of the little group[54] for states along the S direction reveal that for this to occur would require an accidental degeneracy for these bands at the Fermi surface. Shifting E_F towards higher energies to intersect the doubly degenerate state at Z, however, would remove this feature. From our band-structure calculations shown in Fig. 5, we find no available states near E_F with the correct symmetry for an accidental degeneracy to occur indicating an opening of the neck feature along Z. Our results are similar to the APW-LCAO calculations of Mattheiss.[21]

We have also investigated the charge transfer from Ru to O by examining the pseudovalence charge-density difference maps within the *independent atom* model.[55] In this model, one defines $\Delta\rho(\mathbf{r})$ as the difference between the total valence electron density and a linear superposition of radially symmetric atomic charge densities. In regions of positive deformation, charge accumulation occurs and corresponds to "bonding" electrons, while regions of negative deformation, where charge depletion occurs, corresponds to "antibonding" states.

In Fig. 9 we show contours of the pseudovalence charge-density deformation maps in the (110) and ($\bar{1}$10) planes of the tetragonal unit cell. Solid and dashed contours correspond to regions of charge accumulation and depletion, respectively. We have calculated $\Delta\rho$ using the same spherical pseudoatomic charge densities used in constructing the ion core *ab initio* pseudopotentials. The most prominent feature in these figures is the substantial degree of charge transfer along the Ru-O bonds and the charge accumulation along the Ru-Ru bonds perpendicular to the c axis. This is a substantially different picture than that obtained from the charge contained within the Wigner-Sietz radii centered about each atom as pointed out in the LMTO calculations of Xu, Jarlborg, and Freeman.[22] As noted by these authors, this is a result of the commonly accepted yet idealistic ionic model. Figure 9 clearly shows, however, that charge-transfer effects in transition-metal oxides are more complicated.

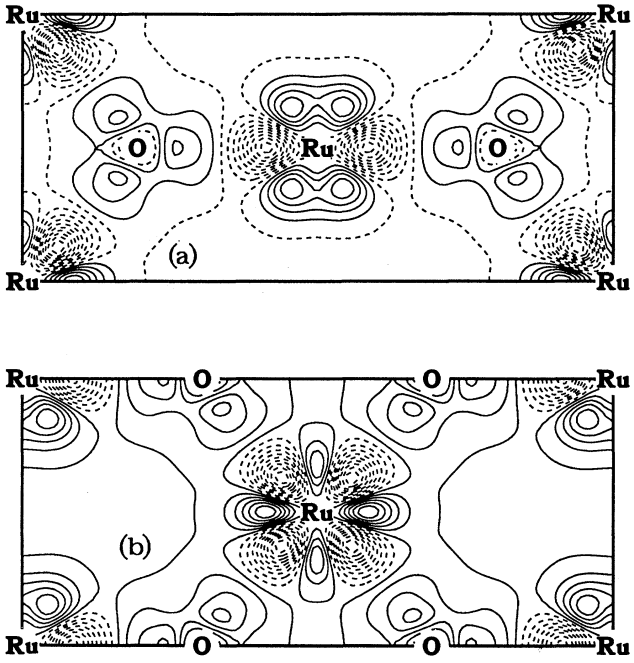

FIG. 9. Pseudovalence charge-density difference maps for the (a) (110) and (b) ($\bar{1}$10) lattice planes. Contours of constant charge density are separated by $6\,e/V_0$.

Our total pseudovalence charge density is virtually identical to the contour plots of the valence charge density obtained from the FLAPW calculations of Sorantin and Schwarz[24] [Fig. 8(c)]. Such good agreement rein-

TABLE V. X-ray structure factors, in electrons per unit cell, for the total charge density compared to the all-electron FLAPW calculations of Sorantin and Schwarz (Ref. 24) and experimental results by Boman (Ref. 43) for various low-index **G** vectors. Theoretical structure factors are the sum of the pseudovalence and core-electron structure factors; the core contributions were calculated from the all-electron calculations used in generating our pseudopotentials. The sign of the experimental structure factors was chosen to be consistent with theory.

	Present work				Experiment
hkl	Core	Valence	Total	FLAPW	F_{obs}
110	68.08	9.26	77.34	77.57	77
101	62.15	−0.49	61.66	62.01	69
200	57.10	−6.75	50.35	50.77	59
111	−6.91	−11.80	−18.71	−18.74	−23
210	4.72	7.36	12.08	12.11	12
211	60.09	3.52	63.61	64.25	53
220	61.30	5.52	66.82	67.48	58
002	64.00	8.22	72.22	72.95	76
301	59.66	4.69	64.36	65.15	59
400	49.83	0.0	49.83	50.50	46
330	52.60	1.44	54.04	54.80	48
004	46.04	0.03	46.08	46.63	43

forces the association of our pseudovalence charge density with the true valence electron density for regions away from the core. This can be seen in Table V, where we list the x-ray structure factors, in electrons per unit cell, for the total charge density compared to the all-electron FLAPW calculations of Sorantin and Schwarz[24] and the experimental results of Boman[43] for various low-index G vectors. The sign of the experimental x-ray structure factors were chosen to agree with theoretical calculations. The present x-ray structure factors were calculated from the sum of the pseudovalence structure factors, obtained from our total-energy calculations, and the core contributions. The core contribution to the x-ray structure factors, as given by the Fourier transform of the core charge, were taken from the all-electron calculations used in generating our pseudopotentials. Core and valence contributions are also listed separately in Table V. The major contribution to the total structure factor results from core contributions. As the dominant contribution is a result of Ru core states, we have tested various excited-state configurations and found no significant changes in the Ru core contributions.

As seen in Table V, our pseudopotential results are in good agreement with the all-electron FLAPW results of Sorantin and Schwarz,[24] the difference being approximately 1% lower for the tabulated values. Although the theoretical calculations represent static structure factors, i.e., frozen-core approximation, they are in reasonable agreement with experiment,[43] considering that inelastic scattering and temperature effects have not been included in the theoretical values as well as the exclusion of thermal diffuse scattering corrections in the experimental intensities. However, these effects tend to lower the observed intensities and would bring the theoretical and experimental structure factors in closer agreement. We have not attempted to remove these effects from experiment as valence and semicore deformations in the charge density would be model dependent as apparent from the charge deformation maps of Fig. 9.

V. SUMMARY

We have calculated the electronic and structural properties of metallic RuO_2 within the local-density approximation. We have employed soft-core *ab initio* pseudopotentials in conjunction with a plane-wave basis and a fast iterative diagonalization technique. We find good agreement with experimentally determined structural properties, i.e., within 2% or better, as well as with pressure-induced structural changes.[46] Our cohesive energy is within 10% of the experimentally determined value, as is typical of the local-density approximation. The electronic properties are found to be in good agreement with experimental photoemission measurements with respect to bandwidths and peak positions. Our theoretically determined Fermi surface is found to be in good agreement with models determined from experimental extremal areas for closed orbits. We also examined the pseudovalence charge density in the independent atom model. Our results indicate good results are obtainable for the structural and electronic properties of late transition-metal oxides within the local-density approximation for *weakly magnetic* systems.

ACKNOWLEDGMENTS

We would like to acknowledge support for this work by the Division of Materials Research, Office of Basic Energy Sciences, U.S. Department of Energy, under Grant No. DE-FG02-89ER45391 and by the Minnesota Supercomputer Institute.

[1]W. D. Ryden, A. W. Lawson, and C. C. Sartain, Phys. Rev. B **1**, 1494 (1970).

[2]A. T. Ashcroft, A. K. Cheetham, J. S. Foord, M. L. H. Green, C. P. Grey, A. J. Murrell, and P. D. F. Vernon, Nature **344**, 319 (1990).

[3]N. C. Halder, Electrocomp. Sci. Technol. **11**, 21 (1983); K. Bobran and A. Kusy, J. Phys. Condens. Matter **3**, 7015 (1991).

[4]D. R. Craig, European Patent No. 82109061 (1983).

[5]G. Blondeel, A. Harriman, G. Porter, D. Urwin, and J. Kiwi, J. Phys. C **87**, 2629 (1983); A. Mills and N. McMurray, J. Chem. Soc. Faraday Trans. 1 **84**, 379 (1988), and references therein.

[6]S. Trasatti, Electrochim. Acta **36**, 225 (1991).

[7]S. Trasatti and W. E. O'Grady, in *Advances in Electrochemistry and Electrochemical Engineering*, edited by H. Gerischer and C. W. Tobas (Wiley-Interscience, New York, 1981), Vol. 12, p. 177.

[8]D. M. Novak, B. V. Tilak, and B. E. Conway, in *Modern Aspects of Electrochemistry*, edited by J. O'M. Bockris, B. E. Conway, and R. E. White (Plenum, New York, 1982), Vol. 14, p. 195.

[9]R. Kötz and S. Stucki, Electrochim. Acta **31**, 1311 (1986).

[10]E. R. Kötz and S. Stucki, J. Appl. Electrochem. **17**, 1190 (1987).

[11]K. M. Glassford and J. R. Chelikowsky, Phys. Rev. B **46**, 1284 (1992).

[12]J. E. Graebner, E. S. Greiner, and W. D. Ryden, Phys. Rev. B **13**, 2426 (1976).

[13]R. T. Slivka and D. N. Langenberg, Phys. Lett. **28A**, 169 (1968).

[14]S. M. Marcus, Phys. Lett. **28A**, 191 (1968).

[15]S. M. Marcus and S. R. Butler, Phys. Lett. **26A**, 518 (1968).

[16]J. Riga, C. Tenret-Noël, J. J. Pireaux, R. Caudano, J. J. Verbist, and Y. Gobillon, Phys. Scr. **16**, 351 (1977).

[17]N. Beatham and A. F. Orchard, J. Electron Spectrosc. Relat. Phenom. **16**, 77 (1979).

[18]R. R. Daniels, G. Margaritondo, C.-A. Georg, and F. Lévy, Phys. Rev. B **29**, 1813 (1984).

[19]P. A. Cox, J. B. Goodenough, P. J. Tavener, D. Telles, and R. G. Egdell, J. Solid State Chem. **62**, 360 (1986).

[20]A. K. Goel, G. Skorinko, and F. H. Pollak, Phys. Rev. B **24**, 7342 (1981).

[21]L. F. Mattheiss, Phys. Rev. B **13**, 2433 (1976).

[22]J. H. Xu, T. Jarlborg, and A. J. Freeman, Phys. Rev. B **40**, 7939 (1989).

[23]K. Schwarz, Phys. Chem. Miner. **14**, 315 (1987).
[24]P. I. Sorantin and K. Schwarz, Inorg. Chem. **31**, 567 (1992).
[25]P. Hohenberg and W. Kohn, Phys. Rev. **136**, B864 (1964); W. Kohn and L. J. Sham, *ibid.* **140**, A1133 (1965).
[26]*Theory of the Inhomogeneous Electron Gas,* edited by S. Lundqvist and N. H. March (Plenum, New York, 1983); W. E. Pickett, Comput. Phys. Rep. **9**, 115 (1989); R. O. Jones and O. Gunnarsson, Rev. Mod. Phys. **61**, 689 (1989).
[27]O. H. Nielsen and R. M. Martin, Phys. Rev. Lett. **50**, 697 (1983); Phys. Rev. B **32**, 3780 (1985); **32**, 3792 (1985).
[28]S. Fahy, X. W. Wang, and S. G. Louie, Phys. Rev. Lett. **61**, 1631 (1988).
[29]A. Svane and O. Gunnarsson, Phys. Rev. Lett. **65**, 1148 (1990); M. R. Norman, Int. J. Quantum. Chem. Symp. **25**, 431 (1991).
[30]J. L. Martins, N. Troullier, and S.-H. Wei, Phys. Rev. B **43**, 2213 (1990).
[31]N. Troullier and J. L. Martins, Phys. Rev. B **43**, 1993 (1991).
[32]A. Rappe, K. Rabe, E. Kaxiras, and J. D. Joannopoulos, Phys. Rev. B **41**, 1227 (1990); D. Vanderbilt, *ibid.* **32**, 8412 (1985).
[33]R. Car and M. Parrinello, Phys. Rev. Lett. **55**, 2471 (1985).
[34]J. L. Martins and M. L. Cohen, Phys. Rev. B **37**, 6134 (1988).
[35]K. M. Glassford, N. Troullier, J. L. Martins, and J. R. Chelikowsky, Solid State Commun. **76**, 635 (1990).
[36]D. M. Ceperley and B. J. Adler, Phys. Rev. Lett. **45**, 566 (1980).
[37]J. P. Perdew and A. Zunger, Phys. Rev. B **23**, 5048 (1981).
[38]L. Kleinman, Phys. Rev. B **21**, 2630 (1980); G. B. Bachelet and M. Schlüter, *ibid.* **25**, 2103 (1982).
[39]L. Kleinman and D. M. Bylander, Phys. Rev. Lett. **48**, 1425 (1982).
[40]X. Gonze, P. Käckell, and M. Scheffler, Phys. Rev. B **41**, 12 264 (1990); D. R. Hamann, *ibid.* **40**, 2980 (1989); X. Gonze, R. Stumpf, and M. Scheffler, *ibid.* **44**, 8503 (1991); D. M. Bylander and L. Kleinman, *ibid.* **41**, 907 (1990).
[41]C.-L. Fu and K.-M. Ho, Phys. Rev. B **28**, 5480 (1983).
[42]D. B. Rogers, R. D. Shannon, A. W. Sleight, and J. L. Gillson, Inorg. Chem. **8**, 841 (1969).
[43]C.-E. Boman, Acta Chem. Scand. **24**, 116 (1970).
[44]F. Birch, J. Geophys. Res. **57**, 227 (1952); F. D. Murnaghan, Proc. Natl. Acad. Sci. U.S.A. **30**, 224 (1944).
[45]O. Gunnarsson, B. I. Lundqvist, and J. W. Wilkins, Phys. Rev. B **10**, 1319 (1974).
[46]R. M. Hazen and L. W. Finger, J. Phys. Chem. Solids **42**, 143 (1981).
[47]*CRC Handbook of Chemistry and Physics,* 73rd ed. (Chemical Rubber, Boca Raton, 1992).
[48]C. Kittel, *Introduction to Solid State Physics,* 6th ed. (Wiley, New York, 1986).
[49]G. Lehmann and M. Taut, Phys. Status Solidi **54**, 469 (1972); O. Jepsen and O. K. Anderson, Solid State Commun. **9**, 1763 (1971).
[50]G. K. Wertheim, L. F. Mattheiss, M. Campagna, and T. P. Pearsall, Phys. Rev. Lett. **32**, 997 (1974).
[51]J. J. Yeh and I. Lindau, At. Data Nucl. Data Tables **32**, 1 (1985).
[52]B. C. Passenheim and D. C. McCollum, J. Chem. Phys. **51**, 320 (1969).
[53]J. M. Ziman, *Electrons and Phonons,* 2nd ed. (Oxford University Press, Oxford, 1979).
[54]J. G. Gay, W. A. Abers, Jr., and F. J. Arlinghaus, J. Phys. Chem. Solids **29**, 1449 (1968).
[55]F. L. Hirshfeld, Isr. J. Chem. **16**, 226 (1977).